Comparison of Cooling Methods for Underground Electric Vehicle Chargers

Shinde, Siddhesh; Mouli, Gautham Ram Chandra; Falsetti, Chiara; Bauer, Pavol

DOI
10.1109/ITherm55375.2024.10709528

Publication date
2024

Document Version
Final published version

Published in
Proceedings of the 23rd IEEE Intersociety Conference on Thermal and Thermomechanical Phenomena in Electronic Systems, ITherm 2024

2024 23rd IEEE Intersociety Conference on Thermal and Thermomechanical Phenomena in Electronic Systems (ITherm) | 979-8-3503-6433-0/24/$31.00 ©2024 IEEE | DOI: 10.1109/ITherm55375.2024.10709528

Comparison of Cooling Methods for Underground Electric Vehicle Chargers

Siddhesh Shinde, Gautham Ram Chandra Mouli, Chiara Falsetti, Pavol Bauer
Delft University of Technology
s.s.shinde-1@tudelft.nl

***Abstract*—This paper compares the indirect cooling method using a heatpipe and air-cooled circular fins with conventional cooling methods like forced air convection and forced water convection for cooling power electronics placed underground. A two-module dual active bridge power converter with reconfigurable outputs for electric vehicle charging is used for the thermal analysis. The comparison is based on specific constraints imposed by semiconductor switch surface area requirements and the maximum junction temperature limit. A detailed analysis is presented, and performance parameters like convective resistance, pressure drop, and mechanical pumping power of the cooling systems as the function of volume flow of working fluid are obtained. Commercially available cooling components like extruded fin heatsinks, cold plate, and heat exchanger are used for conventional cooling methods analysis. Whereas indirect cooling using heatpipes and air-cooled circular fins is designed by performing individual analysis on a heatpipe sizing, air-cooled circular fin design, and heatpipe integrated base plate. This work also highlights the equivalent thermal resistance model for each cooling system.**

***Index Terms*—Heatpipes, underground power electronics, thermal resistance, thermal management, thermal analysis of power electronics**

I. Introduction

Placing sizable power converters for electric vehicle (EV) chargers underground is primarily done in facilities where space is constrained. High-power EV chargers with large footprints occupy a significant amount of space in parking areas. This limits the available parking space and compromises vehicle maneuverability. Therefore, the utilization of underground converters facilitates saving space.

In contrast to the power converter placed above the ground, underground power converters are preferred to be sealed to protect from dust and water ingress, making heat dissipation from them challenging. Additionally, power electronics semiconductor components like MOSFETs and SiCs have high heat flux and require a component-level cooling mechanism to ensure that the junction temperature of the switch is within a safe operating area. Therefore, for the reliable operation of the power converter, heat dissipation from the underground placement of the power converter needs to be managed effectively.

Limited attention has been given to the thermal management of the power electronics when placed underground. One specific study [2] shows the packaging and thermal modeling of wireless charger coils and power electronics for in-road installation. This study typically deals with cooling power converters using neighboring soil. The cooling performance is seen as dependent on the load profile and thermal conductivity of the surrounding soil, which varies with environmental conditions. To remove this dependency and unpredictability of cooling performance, the present work focuses on cooling methods that dissipate heat into the air. Electronics cooling methods are generally classified based on heat flux attainable at specified temperature differences [1]. In addition to this, other considerations like power consumption, volume, cost, and maintenance of the cooling system can also influence the decision to select a cooling method.

In practice, widely used cooling methods for power electronics thermal management are based on forced air convection cooling with heatsinks and forced liquid convection cooling using cold plates. Literature [3]–[6] highlights the usefulness and advances of these basic cooling methods in power electronics. Apart from these two cooling methods, a promising indirect cooling method using two-phase cooling technology has been investigated in recent years. Devices like heat pipes, thermosyphon systems, and micro-channels evaporators have been developed for cooling electronics [13]–[15] and high power electronics [7], [8]. In two-phase cooling, latent heat of vaporization is exploited to transport heat over long distances with a corresponding small temperature difference [9]. Consequently, indirect cooling using a two-phase cooling technology can be a potential cooling method for underground power electronics installations. It can transfer high heat load into the air without the need for vents and allow the sealing of the underground power electronics.

In this work, only the DC-DC part of the EV charger is considered for thermal analysis. A 25kW Two-module reconfigurable Dual Active Bridge (DAB) topology is used. Conventional cooling methods like forced air convection and forced water convection are compared to an indirect cooling method using heatpipes and air-cooled circular fins. These cooling methods are designed to restrict the maximum junction temperature to 120°C, and the temperature variation of other components like power inductors, power transformers, and filter capacitors are not considered in this thermal design. The study aims to present analytical equations to calculate each cooling method's convective thermal resistance and pressure drop characteristics. The thermal resistance models are also presented to show the heat flow paths. Finally, a qualitative

The project was carried out with a Top Sector Energy subsidy from the Ministry of Economic Affairs and Climate, carried out by the Netherlands Enterprise Agency (RVO). The specific subsidy for this project concerns the MOOI subsidy round 2020.

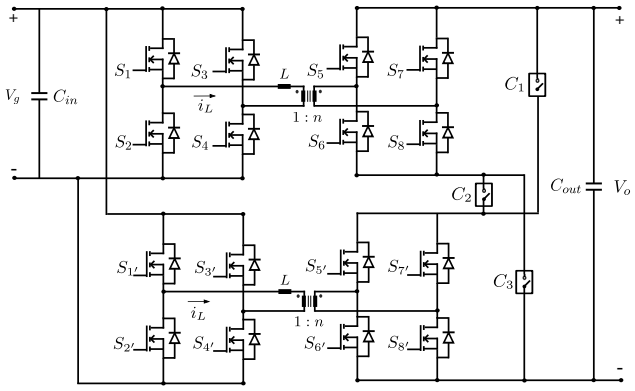

Fig. 1: Two-module Re-configurable Dual Active Bridge.

and quantitative comparison of the cooling method is made based on performance parameters like heat convective transfer coefficient, pressure drop, volume, mechanical pumping power, cost, maintenance, and the possibility of sealing power electronics.

II. Underground EV DC-DC Power converter and losses

Two-module DAB topology with re-configurable outputs, as shown in Fig. 1, is used for cooling method analysis. DAB can be optimally designed for high efficiency at full loads with the help of zero-voltage switching (ZVS) capability. Regardless, when operated at partial powers, the efficiency of the DAB suffers due to operation in non-ZVS region [19].

Each module of the two-module DAB topology operates at 12.5kW power and 750V input voltage V_g . The combined output voltage V_o can be 150V-500V in parallel mode and 300V-1000V in series mode to charge high-voltage EV batteries. Switch C1, C2, and C3 connect modules in parallel or series to obtain the required voltage range. This analysis uses single-phase shift modulation to control the output power.

A. Total losses in switch for EV DCDC converter

Since the design criteria of the cooling system are based on the junction temperature limit, estimating power losses in the primary side and secondary side switches for the entire operating range becomes crucial. Both conduction losses and switching losses given by (1) and (2) are combined to calculate the total loss in the switch Q_{sw-pri} and Q_{sw-sec}. Where $I_{rms,sw}$ is the RMS current in the primary or secondary switch, R_{on} is drain-source resistance when the switch is ON, f_s is switching frequency, and E_{on}, and E_{off} are the tun-on and turn off switching energies respectively.

$$Q_{cond} = I_{rms,sw}^2 R_{on} \tag{1}$$

$$Q_{sw} = (E_{on} + E_{off}) f_s \tag{2}$$

Non-idealities like parasitic capacitance and dead time are ignored, and the ZVS region is based on the current direction at the switching instances [20]. Turn-on switching losses are considered zero when the converter is operated in the ZVS region. Fig. 2 shows the total losses in the single switch on the primary and secondary sides. Due to the identical operation of modules, only one module is considered in the loss analysis.

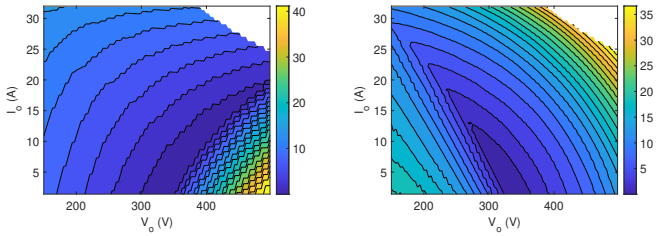

Fig. 2: (a) Q_{sw-pri}, (b) Q_{sw-sec} power loss for entire operating range in Watts

It is observed that the loss distribution in the primary and secondary switches is different, and the worst-case combined primary and secondary switch loss occurs at maximum output voltage and minimum output current set at 5.5A. The combined loss and individual switch loss at this worst-case operating point are shown in Table I. The cooling system design analysis in the following sections is carried out for the condition highlighted in Table I

TABLE I: Losses in DAB switches

Losses	Power	Condition
Single primary switch (Q_{sw-pri})	38 W	V_o: 500V I_o: 5.5A
Single secondary switch (Q_{sw-sec})	15 W	
Switch loss of one module, consisting of 4 primary and 4 secondary switches (Q_{mod})	212 W	
Total switch loss for two modules (Q_{tot})	424 W	

B. Switch thermal model and geometry

A simple thermal resistance model consisting of a junction to the case thermal resistance R_{jc} and case to heatsink or cold plate surface resistance R_{cs} is used to represent 1D heat flow in switch and thermal interface layer (TIM). Both primary and secondary side switches are identical, and R_{jc} value of 0.46 $°C/W$ is specified in the datasheet of C3M0016120K SiC, for the TO-247 package using a thermal conductive gel sheet as TIM, R_{cs} is 0.4 $°C/W$.

For the worst-case loss of 38W, as observed in the single primary switch from Table I, the maximum surface temperature of sink or cold plate $T_{s,max}$ is calculated as 87.3$°C$, assuming junction temperature is restricted to 120$°C$.

There are a total of 16 switches in a two-module DAB converter. 8 on the primary side and 8 on the secondary side. The minimum area, including the headroom for all 16 switches, is 165mm x 150mm. The maximum surface temperature $T_{s,max}$ and switch surface area impose the constraints for designing and selecting cooling system components.

III. Forced air Convection Cooling for Underground Power Electronics

Cooling underground power electronics using forced air convection is challenging due to the enclosed space where maintaining good airflow can be difficult. Underground enclosures cannot have open vents or louvers on the sides as all the surfaces except the top of the underground enclosures are in contact with the soil. Therefore, guided airflow with filters is required to bring atmospheric air from the top surface with limited dust and water ingress.

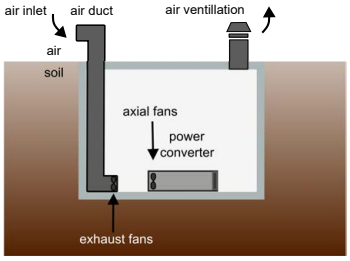

Fig. 3: Forced air convection cooling of underground power electronics.

Fig. 3 shows the cooling of underground power electronics using forced air convection. Here, two heat transfer mechanisms are utilized. Underground enclosure ventilation and forced convection cooling for power electronic components. The primary objective of ventilation is to displace the air inside the underground enclosure by pressurizing the enclosure. In comparison, forced convection cooling primarily improves the convective heat transfer rate and reduces component temperatures. In the following section, both these cooling mechanisms are analyzed considering the ambient temperature of T_a 32°C, which is equivalent to the inlet temperature T_i for the underground enclosure.

A. Underground enclosure ventilation

The underground enclosure is ventilated using the duct with the exhaust fan. The exhaust fan displaces the air inside the underground enclosure with the help of the vent connected to the top surface. The exhaust fan flow rate can be estimated based on the conservation of energy equation for the steady flow of fluid in the tube given by (3) [1]

$$\dot{Q} = \dot{m} c_p (T_e - T_i) \tag{3}$$

Where $\dot{Q}$ is the rate of heat transfer to the fluid and T_i, and T_e are the mean fluid temperature at the inlet and outlet, respectively. $\dot{m}$ is mass flow rate and c_p is specific heat capacity of the fluid. The bulk temperature within an enclosure refers to the average air temperature. The bulk mean temperature inside the tube is the arithmetic mean of the inlet and outlet temperature given by the (4) [1]

$$T_b = (T_e + T_i)/2 \tag{4}$$

Based on (3) and (4), the bulk mean temperature for different flow rates is obtained for inlet temperature of 32°C and power dissipation of Q_{tot} as shown in Fig. 4(a). The

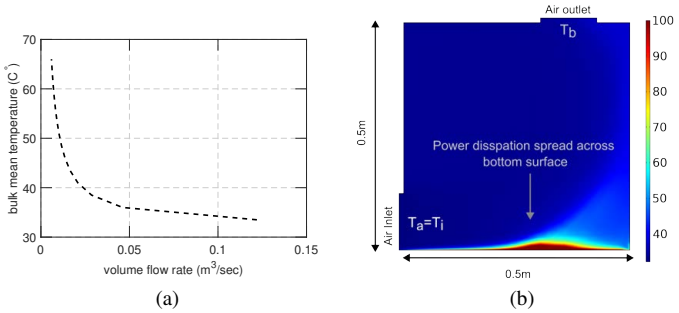

(a) (b)

Fig. 4: (a) Bulk mean air temperature with respect to the volume flow rate of the air, (b) Surface temperature FEM simulation of 2-D Enclosure with perpendicular vent arrangement

higher the volumetric flow rate, the lower the bulk mean fluid temperature inside the enclosure. The conservation of energy given by (3) used to estimate bulk mean fluid inside the tube does not necessarily hold for the enclosure with a cuboid shape with arbitrary inlets and outlets. This can be seen in Fig. 4(b), which shows 2-D enclosures with perpendicular vent arrangement simulated using COMSOL Heat transfer in fluids. The bulk mean temperature is derived by averaging surface area temperatures. The average bulk mean temperature derived is 36.1°C. The loss dissipated is Q_{tot}, inlet temp is 32°C, the flow rate is 0.08 m^3/s, and channel thickness is 0.12 m. Constant power at the bottom surface is assumed as the boundary condition, and the rest of the walls are considered adiabatic.

In practice, the power electronics converter placed on the bottom surface will not act like a constant power heat source. But, it will dissipate losses through forced convection cooling. Based on results obtained from the CFD simulation, it can be deduced that the bulk mean temperature T_b inside the enclosure depends on the following factors:

- Volumetric flow rate of the air.
- Size of the underground enclosure.
- The placement of inlet and outlet vents with respect to the heat source.
- Resistance to airflow caused by the placement of the power converter inside the underground enclosure.

For the design of forced air convection cooling of power electronics components, it is assumed that the bulk mean temperature T_b inside the underground enclosure is maintained and evenly distributed at 35°C by the exhaust fan operating at a flow rate of 0.08 m^3/s based on Fig. 4(a). In practice, baffles, guides, or additional fans inside the underground enclosure can be used to guarantee even air distribution. The bulk mean temperature T_b will be used as an inlet air temperature for the forced convection cooling for power electronics components.

B. Forced air convection cooling for power electronics components

Cooling power electronic components with the help of forced air convection strongly depends on air velocity and the surface area of the heat source [1]. An extruded-fin heatsink

with a fan is utilized as a standard air cooling method to achieve the desired switch junction temperature.

This work uses the composite model from [22] to determine the heat transfer coefficient. This analytical model combines fully developed and developing flow between isothermal parallel plates and is widely used to predict the performance of the heatsink [23].

TABLE II: Extruded fin heatsink parameters

Parameters	Values
Height of heatsink (h_{sink})	0.04 m
Width of the heatsink (w_{sink})	0.0934 m
length of the heatsink (l_{sink})	0.3 m
Height of fins (h_{fin})	0.037 m
Thickness of fins (t_{fin})	0.001 m
Space between fins (s_{fin})	0.002422 m
Number of fins (n_{fin})	28
Length of fins (l_{fin})	0.3 m
Conductivity of heatsink (k_{sink})	238 W/mC
Unfinned surface area (A_{unfin})	0.0196 m^2
Finned surface area (A_{fin})	0.0225 m^2

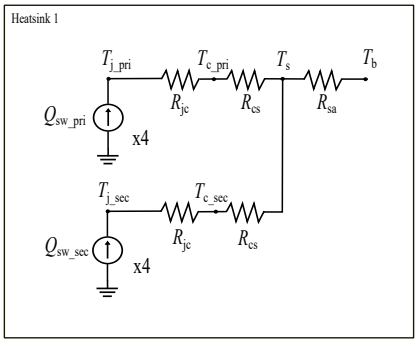

Fig. 5: Equivalent thermal resistance network for forced air convection cooling of power electronics.

Two extruded-fin heatsinks are used, each of dimensions 300mm x 93.4mm x 40mm from Advanced Thermal Solution. Each heatsink consists of one module of DAB converter, i.e., 4 primary and 4 secondary switches. Therefore, loss dissipated by heatsink is Q_{mod} as summarized in Table I. Parameters of the heatsink are specified in Table II [21]. Fig. 5 shows the thermal resistance network for one heatsink.

The model from [23] assumes no spreading resistance and no bypassing of the flow. Equation (5) developed by Teertstra et al. [22] gives the Nusselt number Nu_b from which the heat transfer coefficient for n_{fin} heatsink can be derived. Re_b^* is the channel Reynolds number given by (6) [22], v is kinematic viscosity of air (m^2/s), v_{avg} is the average velocity of air (m/s) and Pr is the Prandtl number.

$$Nu_b = \left[\left(\frac{Re_b^* Pr}{2} \right)^{-3} + \left(0.664 \sqrt{Re_b^*} Pr^{1/3} \sqrt{1 + \frac{3.65}{\sqrt{Re_b^*}}} \right)^{-3} \right]^{1/3} \quad (5)$$

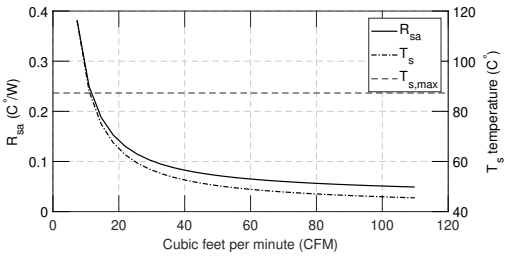

(a)

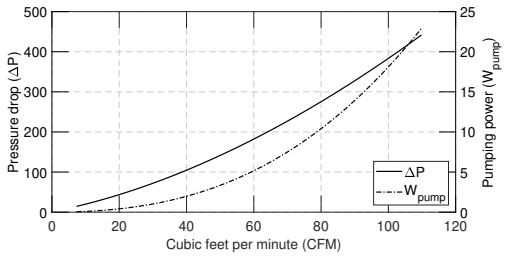

(b)

Fig. 6: (a) Single heatsink convective thermal resistance and surface temperature as a function of air flow rate, (b) Single heatsink air pressure drop as a function of air flow rate.

$$\begin{aligned} \text{Where} \quad & Re_b^* = Re_b \left(\frac{s_{fin}}{l_{fin}} \right) \\ \text{and,} \quad & Re_b = \frac{v_{avg} s_{fin}}{v} \end{aligned} \quad (6)$$

Total heatsink to ambient convective resistance R_{sa} is given by (7) and heat transfer coefficient h by (8).

$$R_{sa} = \frac{1}{h(A_{unfin} + \eta_{fin} n_{fin} A_{fin})} + \frac{h_{sink}}{(k_{sink} w_{sink} l_{sink})} \quad (7)$$

$$h = \frac{Nu_b k_{air}}{s_{fin}} \quad (8)$$

Where, k_{air} is the conductivity of the air (W/mK), and fin efficiency η_{fin} for straight rectangular fin is given by (9) [1]

$$\begin{aligned} \eta_{fin} &= tanh(mh_e)/(mh_e) \\ m &= \sqrt{2h/(k_{sink} t_{fin})} \\ h_e &= h_{fin} + t_{fin}/2 \end{aligned} \quad (9)$$

Finally, the heatsink temperature can be estimated by the (10). Where T_b is considered as 35°C as discussed in Section III-A. Fig. 6(a) gives the surface temperature T_s and convective thermal resistance R_{sa} characteristics with respect to flow rate.

$$T_{sink} = Q_{mod} R_{sa} + T_b \quad (10)$$

The static pressure difference ΔP between the fluid inlet and outlet correlates with the impedance characteristic of the cooling system. ΔP is directly related to the power consumption of the fan or pump to maintain the flow [1] and is analyzed in this section. The pressure difference across

the heatsink is analytically obtained using the models from [23]. This model utilizes the forces balance equation on the heatsink as shown in (11) [24]. Where apparent friction factor f_{app} is for hydrodynamically developing flow is given by (15) [23]. This equation is suitable for estimating pressure drops in power electronic enclosures since the duct is usually non-circular and has a short length. Mechanical pumping power W_{pump} is the product of volume flow rate (m^3/s) and ΔP (N/m^2) [1].

$$\Delta P = \left(\frac{f_{app} n_{fin} (2 h_{fin} l_{fin} + s_{fin} l_{fin})}{h_{fin} w_{sink}} + K_c + K_e \right) \left(\frac{\rho v_{ch}^2}{2} \right) \quad (11)$$

Where ρ is density of air (kg/m^3), v_{ch} is channel velocity and given by (12) [23], K_c and K_e are loss coefficients for sudden expansion and contraction. given by (13) [23]

$$V_{ch} = V_{avg} \left(1 + \frac{t_{fin}}{s_{fin}} \right) \quad (12)$$

$$\begin{aligned} K_c &= 0.42(1 - \sigma^2) \\ K_e &= (1 - \sigma^2)^2 \end{aligned} \quad (13)$$

$$\text{Where} \quad \sigma = 1 - (n_{fin} t_{fin} / w_{sink}) \quad (14)$$

$$f_{app} Re_{Dh} = \left[\left(\frac{3.44}{\sqrt{L^*}} \right)^2 + (f Re_{Dh})^2 \right]^{1/2} \quad (15)$$

$$\begin{aligned} \text{Where} \qquad L^* &= l_{fin} / (D_h Re_{Dh}) \\ Re_{Dh} &= V_{ch} D_h / v \end{aligned} \quad (16)$$

Reference [23] gives the friction factor Reynolds number group to compute fRe_{Dh}. D_h is the hydraulic diameter of the duct and is approximated as $2s_{fin}$ [23]. Fig. 6(b) shows a pressure drop and mechanical pumping power plot as a function of the volume flow of the air for the single heatsink.

IV. Forced liquid Convection Cooling for Underground Power Electronics

Forced liquid convection is usually preferred when the heat flux is about tens of W/cm^2 [3]. Cold plates are typically used to absorb and transfer heat from the component. There are several different types of cold plate technologies, like tube cold plates, fin pin cold plates, and microchannel cold plates [5]. The trend is to increase the surface in contact with the liquid to improve the heat transfer coefficient [5].

In this section, thermal analysis is done using a tube-based cold plate with a tube-fin liquid-to-air heat exchanger. Fig. 7(a) and 7(b) show the placement and block diagram of the close-loop liquid-cooled system. The system has a cold plate on which switches are thermally coupled. A working fluid, in this case, water, moves through the cold plate and absorbs the heat from the components, which is further dissipated into the air using air-to-liquid heat exchangers. A pump is used to circulate the water in the system, and a reservoir is placed to accommodate the expansion-contraction of the working fluid. The same ambient temperature T_a of 32°C as in the case of air convection cooling is assumed.

The analysis uses the cold plate and heat exchanger data from the manufacturer. The goal of the analysis is to ensure that the surface temperature T_s of the cold plate can be maintained lower than $T_{s,max}$ for a known volume flow rate when the system operates in a closed loop. The temperature of the cold plate inlet fluid temperature T_1 cannot be equal to or lower than the ambient temperature T_a. T_1 is chosen as 40°C, which accounts for some headroom over ambient temperature. The single cold plate dissipates the entire power loss Q_{tot}, and no spreading resistance is considered in this analysis. Fig. 8 shows the equivalent thermal resistance network for the cold plate. The outlet temperature of the cold plate T_2 is given by (17).

$$T_2 = \frac{Q_{tot}}{\dot{m} c_p} + T_1 \quad (17)$$

Cold plate maximum thermal resistance $R_{cp,max}$ is given by (18), where the maximum surface temperature of the cold plate surface $T_{s,max}$ is the same as determined in Section II-B.

$$R_{cp,max} = (T_{s,max} - T_2) / Q_{tot} \quad (18)$$

The cold plate is chosen such that its thermal resistance R_{cp} is lower than the calculated maximum thermal resistance $R_{cp,max}$ for the desired flow rate. In this case, $R_{cp,max}$ is 0.10436 °C/W at 2 LPM flow rate when the power dissipated is Q_{tot}. Therefore, 152mm x 177.8mm 6-pass, Hi-Contact cold plate from Aavid manufacturer [25] is chosen, as it meets the required thermal resistance and the switch area criteria given in Section II-B. Fig. 9(a) shows the thermal resistance characteristic of the cold plate, and the data is obtained from the manufacturer.

After selecting the cold plate, the liquid-to-air heat exchanger can be selected based on the capability curve provided by the heat-exchanger manufacturer. The capability curve of the heat exchanger is the function of the volume flow of the liquid in the tube as well as the volume flow of the inlet air. The capability is specified in $W/°C$ which is the amount of the heat removed from the heat exchanger at the given difference between water and air temperature at the inlet of the heat exchnager [1] as shown in (19).

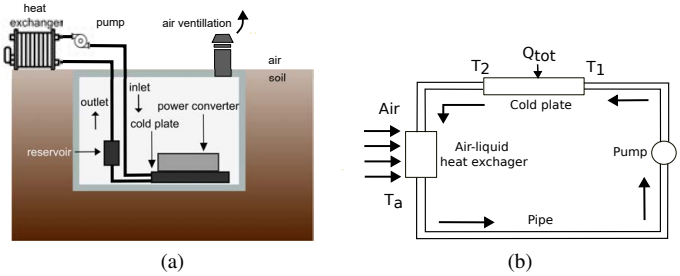

(a) (b)

Fig. 7: (a) Forced liquid convection cooling for underground power electronics, (b) Forced liquid cooling close loop system.

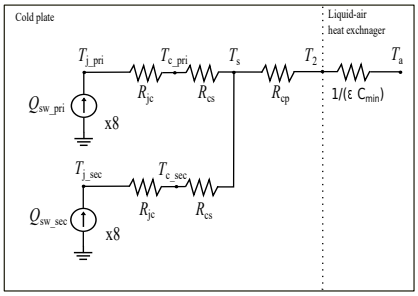

Fig. 8: Equivalent thermal resistance network for forced liquid cooling of power electronics.

$$Capability = \frac{Q_{tot}}{T_2 - T_a} = \varepsilon C_{min} \tag{19}$$

The capability data from the manufacturer is the product of the effectiveness ε of the heat exchanger and minimum heat capacity rate C_{min}. Based on the maximum temperature of the cold plate outlet fluid T_2 derived from (17), ambient temperature T_a, and capability curve, the copper tube-fin heat exchanger M05-100 from Aavid manufacture is selected [26]

To verify if the heat exchanger in a loop with a cold plate can meet the cold plate's surface temperature requirement $T_{s,max}$, (20) is used to plot the surface temperature of the cold plate T_s with respect to flow rate of liquid as shown in Fig. 9(a). Where the variation in R_{cp} with respect to flow rate and εC_{min} is provided by the manufacturer. C_h is the heat capacity rate of the hot fluid, which in this case is water.

$$T_s = Q_{tot}\left[R_{cp} + \left(\frac{1}{\varepsilon C_{min}} - \frac{1}{C_h}\right)\right] + T_a \tag{20}$$

Fig. 9(b) shows the pressure drop of liquid flowing through the cold plate and heat exchanger with respect to the flow rate, and the data is provided by the manufacturer [25], [26]. Fig. 9(b) also shows the mechanical pumping power W_{pump} which in this case is a product of a combined pressure drop of a cold plate and heat exchanger with the volumetric flow of liquid.

To maintain T_1 constant to 40°C, the heat exchanger air-side flow rate of around 160 CFM is required and is obtained from the capability curve given by the manufacturer [26]. The manufacturer also provided the air-side pressure drop data [26]. At 160 CFM, the air-side pressure drop is given as 55 Pa, resulting in the air-side pumping power of 4.15 W.

V. Indirect Cooling Using Heatpipes and Air-Cooled Circular Fins

The heatpipe is a self-contained structure that achieves high thermal energy conductance utilizing two-phase fluid flow with capillary circulation [9]. The latent heat of vaporization is exploited to transport heat over long distances with a corresponding small temperature difference [9]. The effective thermal conductivity of the heat pipe depends on the length, diameter, orientation, working fluid, container, and wick structure. Several other limits govern the heat transport capacity of the heatpipe, viz. capillary limit, sonic, entrainment, viscous, and boiling, and are discussed in [10], [11].

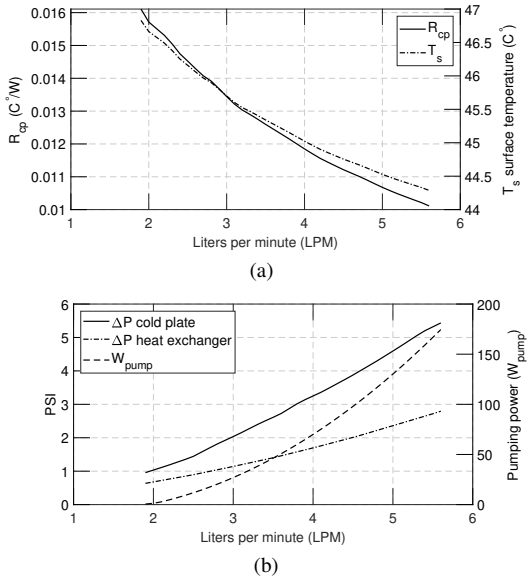

Fig. 9: (a) cold plate thermal resistance and surface temperature as a function of liquid flow rate, (b) cold plate and heat exchanger liquid pressure drop as a function of liquid flow rate

The use of heatpipe is commonly seen in power electronics thermal management. In most applications, heatpipe-embedded heatsinks are used to reduce the thermal spreading resistance [16], [17] and [18]. In some high-power density applications, heatpipes are coupled with magnetic components to transfer the heat to the local heatsink [7], [8]. This section presents a step-by-step design methodology and analysis for the indirect cooling of switches using heatpipes. Fig. 10 shows the structure of the heatpipe integrated power electronics and air-cooled circular fins. The orientation of the heatpipe is vertical, with the condenser section on top connected to circular fins and the evaporator section on the bottom coupled to the switches. In this arrangement, the gravitational force assists the working fluid in flowing from the condenser section to the evaporator section and, therefore, enhances the power-carrying capability of the heatpipe. The length of the evaporator, condenser, and adiabatic section of the heatpipe is shown in Fig. 10.

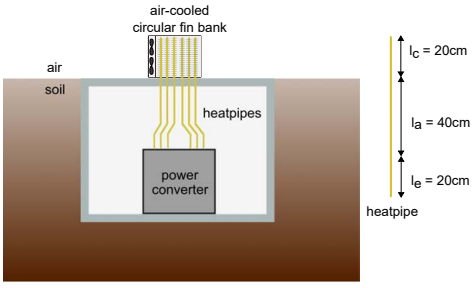

Fig. 10: Indirect cooling using heatpipe and air-cooled circular fins for underground power electronics.

The cooling system design process involves heatpipe design and sizing, heatpipes integrated base plate design, and air-cooled circular fin bank design. The design process is iterative,

and various parameters can be optimized in these individual design steps. In the following sections, each of the design steps and analysis is shown.

A. Heatpipe design and sizing

TABLE III: Heatpipe design parameters.

Parameters	Values
Evaporator length (L_e)	0.2 m
Condenser length (L_c)	0.2 m
Adiabatic length (L_a)	0.4 m
Outer diameter of the pipe (do_p)	0.0127 m
Thickness of the pipe (t_p)	0.8 mm
Inner diameter of the pipe (di_p)	0.0119 m
Vapour diameter (d_v)	0.0109 m
Wire diameter (d_w)	1.143e-04 m
Mesh number (N)	3937 m^{-1}
length of joint (L_j)	0.102 mm
Area of joint (A_j)	0.008 m^2
Pipe wall radial resistance $(R_{p,c}, R_{p,e})$	1.2911e-04 C°/W
Liquid-wick resistance $(R_{w,c}, R_{w,e})$	0.0465 C°/W
Evaporator contact resistance $(R_{ext,e})$	2.556e-04 C°/W
Power carried by each heatpipe (Q_{hp})	70.66 W

The heatpipe's power-carrying capability depends on several factors, as mentioned before. However, a preliminary selection of working fluid, container, and wick structure is required before sizing the heat pipe for the application. There are various resources [10], [11] that highlight the proper selection of these design parameters. This application uses copper-water heatpipes with a two-layer 100 mesh copper screen wick structure.

The sizing of the heatpipe requires the selection of core diameter, wick sizing, and container thickness such that it meets the power-carrying criteria of the heatpipe for the given length, diameter, and orientation [12]. Table III gives the design and sizing parameters of the heatpipe used in this application. In total, six heatpipes are used to transport power Q_{tot} from the base plate to the fins. The selection of the number of heatpipes also depends on the temperature gradient between the evaporator and condenser ends, ΔT, that is proportional to the heatpipe power Q_{hp}, and thermal resistances.

Once the heatpipe design and sizing are defined, the capillary power limit is computed to check if the required heat transport lies below the capillary limit. Fig. 11 shows the capillary limit of the heatpipe with respect to the operating temperature range. This limit is calculated based on the analytical equation provided in [11], which expresses the difference in capillary pressure across the liquid-vapor interface in the evaporator and condenser region. Based on the capillary limit graph, it is verified that the designed heatpipe can carry the Q_{hp} in the estimated operating range of 30°C to 80°C.

The thermal resistance of the heatpipe determines the temperature gradient across it. The simplified thermal resistance network model of heatpipe is used in this analysis, and only the pipe wall radial resistance (21) and liquid-wick resistance (22) at both the evaporator and condenser section is used [11]. The values of these resistances are given in Table III.

$$R_{p,x} = log\frac{(do_p/di_p)}{2\pi L_x k_p} \tag{21}$$

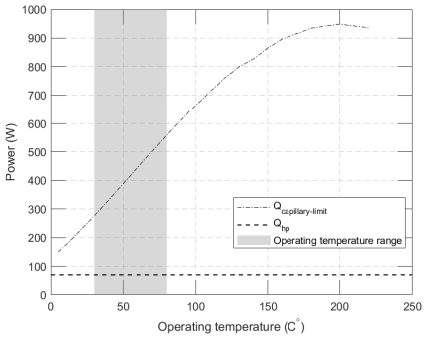

Fig. 11: Capillary limit of the heatpipe with respect to operating temperature.

$$R_{w,x} = log\frac{(do_w/di_w)}{2\pi L_x k_{eff}} \tag{22}$$

where k_{eff} is the effective wick permeability and is given by (23) [11], and L_x is the length of evaporator $L_x = L_e$ or condenser $L_x = L_c$.

$$k_{eff} = \frac{k_l[(k_l + k_w) - (1-\epsilon)(k_l - k_w)]}{[(k_l + k_w) + (1-\epsilon)(k_l - k_w)]} \tag{23}$$

where, ϵ wick porosity for wrapped screen wick is given by (24) [11] and k_l and k_w is the thermal conductivity of liquid and wick material.

$$\epsilon = 1 - (1.05\pi N d_w)/4; \tag{24}$$

B. Air-cooled fins design for the heatpipe condenser section

The heatpipe's condenser surface area can be extended by adding circular or flat fins to the heatpipe. The cross-flow over the finned heatpipe arrays can increase the heat transfer coefficient. This analysis considers aluminum circular fins connected to the heatpipe condenser section. The tubes are arranged staggered in the direction of flow. Fig. 12 shows the staggered tube arrangement. The fins are welded to the heatpipe, and contact resistance is ignored. Table IV shows the design parameters of the circular fins heatpipe arrays.

The correlation used in calculating the heat transfer coefficient is obtained from regression analysis from reference

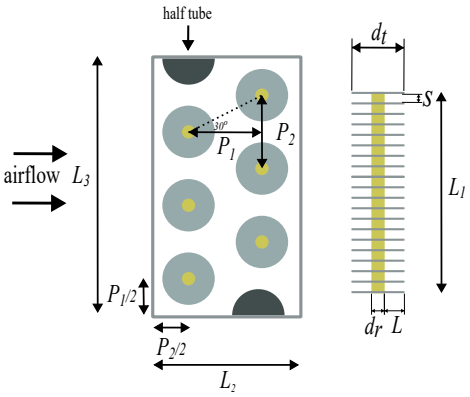

Fig. 12: Circular fins heatpipe staggered array, top and side view.

TABLE IV: circular fin heatpipe array specifications

Parameters	Values
Width of the fins (w)	0.002 m
Root diameter of the fin (D_r)	0.0127 m
Length of the fin (L)	0.02 m
Diameter of the fin tip (D_t)	0.0695 m
Space between the fins (s)	0.008 m
Number of rows (n_r)	2
Transverse distance between the heatpipes ($p1$)	0.07 m
Longitudinal distance between the heatpipes ($p2$)	0.07 m
Fin density (N)	100 m^{-1}
Surface area of the all the fins (A_f)	0.9324 m^2
Surface area of tube between the fins (A_w)	0.0383 m^2
Minimum free flow area (S_{min})	0.0321 m^2
σ is $S_{min}/(L_3L_1)$	0.6562
Height of the bank of heatpipe array (L_1)	0.2 m
longitudinal length of heatpipe array (L_2)	0.14 m
Transverse length of heatpipe array (L_3)	0.245 m
Conductivity of fins (k_{fin})	238 W/mC

[27]. Equation (25) gives a correlation to calculate the average Nusselt number.

$$Nu = 0.242Re^{0.658}Pr^{1/3}\left(\frac{s}{L}\right)\left(\frac{p1}{p2}\right)^{-0.09}F_1F_2 \quad (25)$$

This correlation is valid for the following conditions [27]:

- $2000 < Re < 40{,}000$
- $0.13 < s/L < 0.57$
- $1.15 < p1/p2 < 1.72$

Where Reynolds number Re is given by (26), F_1 incorporates variation in the fluid property and is given by Prandtl number evaluated at bulk temperature Pr_{bulk}, and heatpipe wall temperature Pr_{wall}. F_1 is calculated as $(Pr_{bulk}/Pr_{wall})^{0.26}$ and F_2 is a correction factor and is 0.84 for two rows [27].

$$Re = \frac{v_{max}D_r}{\nu} \quad (26)$$

Where v_{max} is the maximum velocity evaluated at the minimum free flow area given by (27)

$$v_{max} = \frac{\dot{m}}{\rho S_{min}} \quad (27)$$

Circular fin heatpipe array to ambient convective resistance R_{ha} is obtained from (28)

$$R_{ha} = \frac{1}{h(A_w + \eta_{fin}A_f)} \quad (28)$$

Where h is the convective heat transfer coefficient calculated for the entire array and is given by (29) [27] and η_{fin} is the fin efficiency and is given by(30), [27].

$$h = \frac{Nuk_{air}}{D_r} \quad (29)$$

$$\begin{aligned} \eta_{fin} &= tanh(m\theta)/(m\theta) \\ m &= \sqrt{2h/(k_{fin}w)} \\ \theta &= \frac{D_r}{2}\left(\frac{D_t}{D_r} - 1\right)\left(1 + 0.35log\left(\frac{D_t}{D_r}\right)\right) \end{aligned} \quad (30)$$

The flow over the tube bank, in this case, the heatpipe array, is considered as internal flow [1]. For the constant surface heat flux boundary condition on heatpipes and circular fins, the maximum surface temperature of the heatpipe array can be computed at the exit of the array. Equation (31) gives the maximum surface temperature of the heatpipe array. Here, the exit temperature of the heatpipe array T_e is based on the conservation of energy, given by (3).

$$T_{fin,array} = T_e + Q_{tot}R_{ha} \quad (31)$$

Fig. 13(a) shows the variation of convective resistance of circular fin heat pipe array R_{ha} as well as shows the surface temperature variation of heatpipe fins array $T_{fin,array}$ with respect to the volume flow of the air.

The pressure loss calculation across the circular fin heatpipe arrays is obtained from correlation from reference [28]. Equation (32) gives the total static pressure loss for the array [28].

$$\Delta P = (k_a + n_r k_f)\frac{\rho v_{max}^2}{2} \quad (32)$$

Where k_a is the pressure loss due to acceleration and is given by (33), whereas k_f is the pressure loss due to friction as is given by (34) [28].

$$k_a = 1 + \sigma^2 \quad (33)$$

$$K_f = 4.71Re^{-0.286}\left(\frac{L}{s}\right)^{0.51}\left(\frac{p1 - D_r}{p2 - D_r}\right)^{0.536}\left(\frac{D_r}{p1 - D_r}\right)^{0.36} \quad (34)$$

The correlation in the (34) is valid for the following conditions [28]:

- $10^3 \leq$ Re $\leq 10^5$,
- $1.54 \leq$ L/s ≤ 5.67
- $1.18 \leq (p1 - D_r)/(p2 - D_r) \leq 2.07$
- $0.13 \leq D_r/(p1 - D_r) \leq 2.86$

Fig. 13(b) shows the static pressure drop across the heatpipe circular fin array as well as mechanical pumping power W_{pump} as the function of the volume flow of air.

C. Heatpipe integrated base plate

Aluminum baseplate of length l_{base} of 200mm, width w_{base} of 150mm, and height h_{base} of 40mm is used based on the criteria given in Section II-B. This base plate incorporates 6 heatpipes, and the interface consists of Solder 63Sn/37Pb with effective thermal conductivity of 50 $W/m°$C. The contact resistance at the evaporator is given by the (35).

$$R_{ext,e} = L_j/(k_j A_j) \quad (35)$$

Where L_j is the length of the joint and A_j is the area of the joint as mentioned in Table III. The thermal resistance of the base plate accounts for the heat flow path between the surface

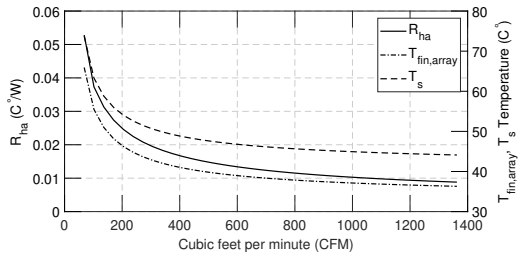

(a)

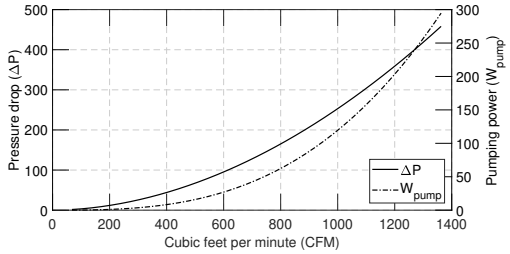

(b)

Fig. 13: (a) Heatpipe array thermal resistance, fin array surface temperature and base plate surface temperature as a function of air flow rate, (b) Static pressure drop across circular fin heatpipe array as a function of air flow rate.

area of switches and the heatpipe given by (36), assuming that the heatpipes arrays are placed at the center of the base plate.

$$R_{base} = \frac{(h_{base}/2)}{(k_{base} l_{base} w_{base})} \tag{36}$$

Where k_{base} is the thermal conductivity of aluminum. Once the R_{base} is known, the surface temperature of the heatpipe integrated baseplate can be computed and is shown in Fig. 13(a) as variation in T_s with respect to the volume flow rate of air.

The equivalent thermal resistance network for the indirect cooling of power electronics using heatpipes and circular fins is shown in Fig. 14.

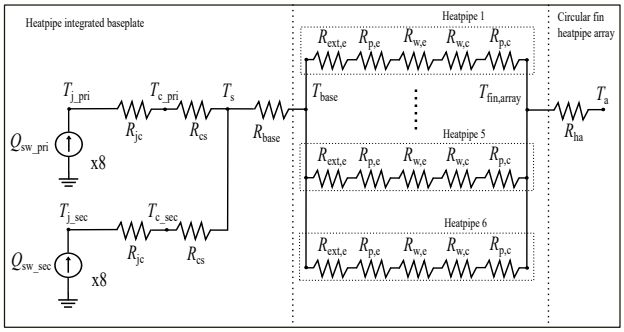

Fig. 14: Equivalent thermal resistance network for indirect cooling using heatpipe and circular fin array.

VI. Comparison of cooling methods for underground power electronics

The cooling methods are designed for specific constraints like the surface area requirement of the switches and the maximum junction temperature limit of the switches. The quantitative comparison is done based on the pressure drop, heat transfer convective resistance, mechanical pumping power, and the volume of the cooling system. Whereas, The qualitative comparison is based on cost, maintenance, and the ability to isolate power electronics from the external environment by sealing. The cooling system's performances are evaluated for surface temperature T_s of 46°C. This limit is far below the $T_{s,max}$ and is chosen because this is the temperature a liquid-cooled system can achieve at a minimum flow rate based on the data provided by the manufacturer. The following section gives the details of how these performance parameters are evaluated, and they are highlighted in Table V.

A. Performance parameters of air-cooled system

The performance parameters of the underground ventilation system are not evaluated, but its effect on bulk mean temperature T_b is used as inlet air temperature for deriving the performance parameters of forced air convection cooling as discussed in Section III-B. The performance parameters are evaluated when heatsink temperature T_s is maintained at 46°C.

- T_s of 46°C is achieved at 98 CFM rate for one heatsink.
- Convective heat transfer resistance R_{sa} of 0.0514°C/W.
- Pressure loss ΔP for one heatsink is 373 Pa.
- Pumping power required W_{pump} of 17.2W for one heatsink. For two heatsink W_{pump} is 34.4W
- Dimension of one heatsink [21]: 0.3m x 0.0934m x 0.04m, combined volume of two heatsinks: $0.00224 m^3$. Volume comparison excludes air duct and fan.

B. Performance parameters of water-cooled system

For the water-cooled convection cooling design based on Section IV, the following performance is achieved when T_s of cold plate is maintained at 46°C.

- T_s of 46°C is achieved at 2.6 LPM rate.
- Convective heat transfer resistance R_{cp} of 0.0143°C/W.
- Pressure loss ΔP for cold plate: 1.5 PSI and ΔP for heat exchanger: 0.943 PSI, combined ΔP is 2.443 PSI.
- Pumping power required W_{pump} 14.48W, and heat exchanger air-side W_{pump} is 4.15W. The combined pumping power is 18.63W
- Dimension of cold plate [25]: 0.152m x 0.1778m x 0.014m, dimensions of heat exchanger [26]: 0.16m x

TABLE V: Comparison of cooling methods.

Parameters	Forced air cooling	Forced liquid cooling	Indirect cooling
Convective resistance	0.0514°C/W	0.0143°C/W	0.0122°C/W
Pressure drop	373 Pa	2.443 PSI (16.8 kPa)	133.3 Pa
Pumping power	34.4W	18.63W	45W
Volume	0.00224 m^3	0.00507 m^3	0.00188 m^3
Maintenance	low	high	low
Cost	low	high	high
Sealing of power electronics	No	Yes	Yes

0.0889m x 0.33m. Combined volume: $0.00507m^3$. Volume comparison excludes connecting pipes and water pump.

C. Performance parameters of indirect cooled system

For the indirect cooling using heatpipe and air-cooled circular fin design based on Section V, the following performance is achieved when T_s heatpipe integrated baseplate is maintained at 46°C.

- T_s of 46°C is achieved at 715.4 CFM rate.
- Convective heat transfer resistance R_{ha} of 0.0122°C/W.
- Pressure loss ΔP for circular fin heatpipe array is 133.3 Pa.
- Pumping power required W_{pump} is 45W.
- Dimension of heatpipe integrated base plate: 0.2m x 0.15m x 0.04m, dimensions of circular fin heatpipe array: 0.2m x 0.014m x 0.245m. Combined volume: $0.00188m^3$. Volume comparison excludes heatpipes.

VII. Conclusion

The paper has presented a quantitative and qualitative comparison of three cooling methods - forced air convection cooling, forced water convection cooling, and indirect cooling using heatpipe and air-cooled circular fins for the DCDC part of the EV charger placed underground. The cooling systems are designed to meet the junction temperature limit and surface area requirement of the semiconductor switches. The primary performance parameters, such as convective heat transfer resistance, pressure drop, and mechanical pumping power as the function of working fluid volume flow, are presented. It can be observed that the indirect cooling method has a smaller convective resistance for the given volume of the cooling system, which results in a compact cooling system. Additionally, it can also allow easy sealing of power converters. These are the desirable characteristics of a cooling system for underground EV chargers. The overall cooling performance of the indirect cooling method can be improved by optimizing the design to reduce the pressure drop and thermal resistance from the semiconductor switch case to the surface of the circular fins.

References

[1] Cengel, A. Heat and Mass Transfer: Fundamentals and Applications. (McGraw-Hill Education,2015)

[2] Ridge, A., Konaklieva, S., Bradley, S., McMahon, R. & Kumar, K. Power Electronics Packaging for In-Road Wireless Charging Installations. *2021 IEEE PELS Workshop On Emerging Technologies: Wireless Power Transfer (WoW)*. pp. 1-6 (2021)

[3] Laloya, E., Lucía, Ó., Sarnago, H. & Burdío, J. Heat Management in Power Converters: From State of the Art to Future Ultrahigh Efficiency Systems. *IEEE Transactions On Power Electronics*. **31**, 7896-7908 (2016,11)

[4] Gupta, K., Silva, C., Nasr, M., Assadi, A., Matsumoto, H., Trescases, O. & Amon, C. Thermal Management Strategies for a High-Frequency, Bi-Directional, On-Board Electric Vehicle Charger. *Proceedings Of The 17th InterSociety Conference On Thermal And Thermomechanical Phenomena In Electronic Systems, ITherm 2018*. pp. 935-943 (2018,7)

[5] McPherson, B., McGee, B., Simco, D., Olejniczak, K. & Passmore, B. Direct liquid cooling of high-performance Silicon Carbide (SiC) power modules. *2017 IEEE International Workshop On Integrated Power Packaging (IWIPP)*. pp. 1-5 (2017)

[6] Gammeter, C., Krismer, F. & Kolar, J. Weight optimization of a cooling system composed of fan and extruded-fin heat sink. *IEEE Transactions On Industry Applications*. **51**, 509-520 (2015,1)

[7] Biela, J. & Kolar, J. Cooling concepts for high power density magnetic devices. *Fourth Power Conversion Conference-NAGOYA, PCC-NAGOYA 2007 - Conference Proceedings*. pp. 1-8 (2007)

[8] Pavlovsky, M., Haan, S. & Ferreira, J. Design for Better Thermal Management in High-Power High-Frequency Transformers. (2005)

[9] Zohuri, B. Heat pipe design and technology: Modern applications for practical thermal management, second edition. *Heat Pipe Design And Technology: Modern Applications For Practical Thermal Management, Second Edition*. pp. 1-513 (2016,1)

[10] Chi, S. Heat Pipe Theory and Practice: A Sourcebook. (Hemisphere Publishing Corporation,1976), https://books.google.nl/books?id=nBVkzwEACAAJ

[11] Peterson, G. An Introduction to Heat Pipes: Modeling, Testing, and Applications. (Wiley,1994), https://books.google.nl/books?id=QARIHgRrIVsC

[12] Shah, R., Subbarao, E. & Mashelkar, R. Heat Transfer Equipment Design. (Taylor and Francis,1988), https://books.google.nl/books?id=hQO2utfsk5oC

[13] C. Falsetti, H. Jafarpoorchekab, M. Magnini, N. Borhani, J. R. Thome, "Two-phase operational maps, pressure drop, and heat transfer for flow boiling of R236fa in a micro-pin fin evaporator," Int. J. Heat Mass Transf., vol. 107, pp. 805–819, 2017.

[14] C. Falsetti, M. Magnini, J. R. Thome, "Flow boiling heat transfer and pressure drops of R1234ze(E) in a silicon micro-pin fin evaporator," J. Electron. Packag., vol. 139, 2017.

[15] C. Falsetti, Raffaele L Amalfi, Todd Salamon, Jackson B Marcinichen, J. R. Thome, "Experimental Analysis of the Condenser Design in a Thermosiphon System for Cooling of Telecommunication Electronics," IEEE Transactions on Components, Packaging and Manufacturing Technology, vol. 10, pp. 963–973, 2020.

[16] Wang, Y., Wang, B., Zhu, K., Li, H., He, W. & Liu, S. Energy saving potential of using heat pipes for CPU cooling. *Applied Thermal Engineering*. **143** pp. 630-638 (2018,10)

[17] Wang, Y., Wang, J., He, X. & Duan, J. Experimental investigation of the thermal performance of a heat sink with U-shaped heat pipes. *Applied Thermal Engineering*. **186** (2021,3)

[18] Wang, B., Wang, L., Yang, F., Mu, W., Qin, M., Zhang, F., Ma, D., Wang, J. & Liu, J. Air-Cooling System Optimization for IGBT Modules in MMC Using Embedded O-Shaped Heat Pipes. *IEEE Journal Of Emerging And Selected Topics In Power Electronics*. **9**, 3992-4003 (2021,8)

[19] Mukherjee, S., Kumar, A. & Chakraborty, S. Comparison of DAB and LLC DC-DC Converters in High-Step-Down Fixed-Conversion-Ratio (DCX) Applications. *IEEE Transactions On Power Electronics*. **36**, 4383-4398 (2021,4)

[20] Bhattacharya, S. ABSTRACT MAHADEVA IYER, VISHNU. An Approach Towards Extreme Fast Charging Station Architecture for Electric Vehicles with Partial Power Processing

[21] Advanced Thermal Solutions, INC., "ATS-EXL76-300-R1", https://www.qats.com/Product/Heat-Sinks/Extrusion-Profiles-lengths-/Profiles/ATS-EXL76-300-R1/3349.aspx specifications

[22] Teertstra, P., Yovanovich, M. & Culham, J. Analytical Forced C o nvec t io n Mo deling of Plate Fin Heat Sinks.

[23] Culham, J. & Muzychka, Y. Optimization of Plate Fin Heat Sinks Using Entropy Generation Minimization. *IEEE TRANSACTIONS ON COMPONENTS AND PACKAGING TECHNOLOGIES*. **24** (2001)

[24] Kays, W.M. and London, A.L. (1984) Compact Heat Exchangers. 3rd Edition, McGraw-Hill, New York.

[25] Boydcorp, https://www.boydcorp.com/thermal/liquid-cooling-systems/liquid-cold-plates.html

[26] Boydcorp, https://www.boydcorp.com/thermal/liquid-cooling-systems/heat-exchangers.html

[27] Sabersky, R. & Saunders, E. ESDU 86022 High-fin staggered tube banks: heat transfer and pressure drop for turbulent single phase gas flow THE PREPARATION OF THIS DATA ITEM HIGH-FIN STAGGERED TUBE BANKS: heat transfer and pressure drop for turbulent single phase gas flow CONTENTS.

[28] Mr, C., Taylor, M., Saunders, E. & Taylor, M. ESDU 84016 Low-fin staggered tube banks: heat transfer and pressure loss for turbulent single-phase crossflow THE PREPARATION OF THIS DATA ITEM LOW-FIN STAGGERED TUBE BANKS: heat transfer and pressure loss for turbulent single-phase crossflow CONTENTS. (1984)